Probing Intrinsic Ellipticity in Neutron Star Binaries

Zhiqiang Miao[1] and Huan Yang[2,*]

[1] *Tsung-Dao Lee Institute, Shanghai Jiao Tong University, Shanghai, 201210, China*
[2] *Department of Astronomy, Tsinghua University, Beijing 100084, China*

(Dated: September 2025)

We present a novel resonance mechanism that can naturally occur in neutron star binaries: a spin-orbit resonance. This resonance locks the binary into a unique state where the neutron star spin evolves alongside the orbit. The resonance requires a finite neutron star ellipticity ϵ possibly sourced by strong internal magnetic fields in magnetars, which are motivated by population study of eccentric neutron star-black hole binary GW200105. We find that the locking probability is proportional to $\sqrt{\epsilon}$. We derive the phase correction in the gravitational waveform due to this resonance locking effect, and have conducted a search in all neutron star binaries up to the O4a gravitational-wave catalog, with no positive event found so far. Observations by next-generation detectors such as Einstein Telescope and Cosmic Explorer, or even the upcoming upgrade of Advanced LIGO, have the potential to detect such locking signals, enabling precise measurements of both neutron star's ellipticity and moment of inertia. Future searches should be performed to discover this resonance, or, if undetected, to place constraints on the magnetar fraction in neutron star binaries.

INTRODUCTION

Ten years after the first detection of binary black hole coalescence [1], Gravitational Wave (GW) Astronomy has gradually become a precision science, with physical quantities measured at percentage levels, as particularly celebrated by the loudest event detected so far, GW250114 [2], at the signal-to-noise ratio (SNR) ~ 80. This not only allows for better and more frequent detection of events for population studies, but also the discoveries of small but important effects not necessarily included in current compact-binary templates, such as resonances [3–9], nonlinear ringdowns [10–17], memory [18–24], etc. In this work, we point out an exciting opportunity associated with probing the intrinsic ellipticity of neutron stars.

Neutron stars are generically elliptical, as sourced from the internal magnetic stress. In fact, searching for continuous gravitational waves from rotating pulsars in our own galaxy is one of the science goals of ground-based detectors [25, 26]. On the other hand, measuring star ellipticity ϵ has not been seriously considered previously, partially due to weak coupling of the ellipticity to the waveform, except in the scenario of exotic compact object (ECO) with order-unit deviation from spherical symmetry [27]. We have discovered a novel spin-orbit resonance that naturally takes place in the inspiral stage, locking the evolution of spin and orbit for elliptical stars, providing a much stronger impact on the waveform. Deriving and incorporating the waveform model with such an effect, we find that magnetars within binaries may be discovered by measuring the gravitational waveform alone, together with the determination of their ellipticity and moment of inertia. Interestingly, recent detection of eccentricity in a neutron star-black hole (NSBH) binary [28–30] motivates the existence of magnetars in binaries due to the relatively short ($10^4 - 10^5$ yr) lifetime of the binary [31].

We have performed parameter estimation of all binaries including neutron star up to the O4a GW catalog. The mass-gap event GW190814 shows an interesting peak (corresponding to $\epsilon \sim 10^{-2}$), but statistical evidence is weak. All other events present no signature of this spin-orbit resonance. We find that third-generation (3G) detectors are able to constrain the fraction of magnetars within neutron-star binaries assuming non-detection. In addition, a single detection of an elliptical star likely leads to precise measurements of both the neutron star ellipticity and its moment of inertia, yielding significant implications for both astrophysics and fundamental physics. We adopt the natural unit $c = 1$.

HIERARCHICAL TRIPLE AND MAGNETARS

There is growing evidence that NSBH binaries can have dynamical origins. In particular, of the four NSBH merger events detected so far, there is a recent detection of nonzero eccentricity ($e_{20} \sim 0.145$ at an orbital period of $0.1\,$s) in GW200105 [28–30]. In dense stellar environments, multi-body interactions provide a natural pathway to produce such eccentric merger systems [32–36]. However, they are predicted to produce a merger rate of roughly $\mathcal{R}_{\rm NSBH} \sim 0.1 - 1\,{\rm Gpc}^{-3}\,{\rm yr}^{-1}$, orders of magnitude lower than the rate inferred from gravitational-wave observations. A more compelling explanation for such eccentric mergers is the hierarchical triple scenario [31, 37, 38], in which secular dynamics—most notably the Zeipel–Lidov–Kozai mechanism [39–41]—mediate angular momentum exchange between the inner binary and the outer tertiary, leading to an eccentric fraction in the LIGO band. In addition, recent simulations show that such tertiary-driven NSBH systems can produce a merger rate of $\mathcal{R}_{\rm NSBH} \sim 1 - 23\,{\rm Gpc}^{-3}\,{\rm yr}^{-1}$ [31], consistent with current gravitational-wave observations.

An important aspect of these dynamically assembled systems is that they typically have very short lifetimes. For example, simulations show that the median lifetime of tertiary-driven NSBH systems is approximately $10^4 - 10^5$ yr [31], which is shorter than the timescale over which the internal magnetic field (not the crust field) of a magnetar decays through Ohmic dissipation and Hall drift ($10^5 - 10^6$ yr) [42][43]. Although the birth rate of magnetars remains uncertain, some studies estimate that approximately $1-40\%$ of NS are born as magnetars [44–46]. We therefore argue that a substantial fraction of such tertiary-driven NSBH systems may harbor a neutron star that remains a magnetar at the time of merger, with the neutron star itself sustaining a comparatively large ellipticity induced by magnetic deformation. This ellipticity can be estimated as [47]

$$\begin{aligned}\epsilon &= \kappa \frac{\bar{B}^2 R^3}{GM^2/R} \\ &\approx 4\times 10^{-6}\kappa \left(\frac{1.4\,M_\odot}{M}\right)^2 \left(\frac{R}{12\,\mathrm{km}}\right)^4 \left(\frac{\bar{B}}{10^{15}\,\mathrm{G}}\right)^2 ,\end{aligned} \tag{1}$$

where M and R are the mass and radius of the neutron star, respectively. G is the gravitational constant. $\bar{B}$ represents the volume average of the internal magnetic field. Its value can be much larger than the surface magnetic field strength of magnetars (typically a few times 10^{14} G), and could even reach up to 10^{16} G, especially if a strong toroidal magnetic field is present [48–50]. The parameter κ is of $\mathcal{O}(1)$ and depends on the internal magnetic field geometry and the equation of state (EOS) of the neutron star.

While we have primarily focused on NSBH systems above, it should be noted that the same dynamical channels—both multi-body interactions and hierarchical triples—are also applicable to binary neutron star (BNS) systems [32, 38]. Therefore, we propose that some BNS systems could also harbor magnetars during the inspiral phase. In the following, our analysis will remain focused on NSBH systems, but we also include BNS systems in our injection studies and signal search for existing GW events.

RESONANCE LOCKING, BREAKING, AND WAVEFORM

Consider an NSBH binary with an elliptical neutron star, as illustrated in Fig. 1. For simplicity, we merge the axis of principal inertia and the spin axis, and assume the spin is perpendicular to the orbital plane. We further restrict our discussion to circular orbits. (see Supplementary Material [51] for discussions on the general cases, including arbitrary spin–principal axis orientations and eccentric orbits.). The quadrupole moment of the star

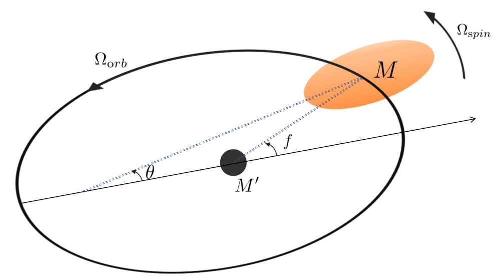

FIG. 1. Schematic diagram of the binary $M - M'$, where the neutron star has a finite ellipticity. The long axis of the neutron star lies in the orbital plane and makes an angle θ with a reference axis fixed in inertial space. f is the true anomaly.

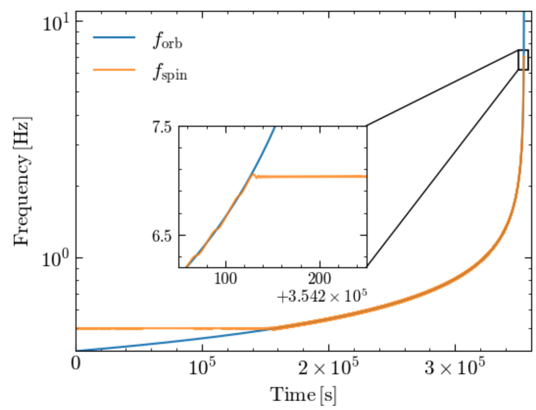

FIG. 2. The evolution of the orbital frequency and neutron star spin frequency with time for a specific locking example, where $M = 1.4\,M_\odot$, $q = 3$, and $\epsilon = 5\times10^{-5}$. The initial phase is set as $f - \theta = 0.3986$.

couples with the tidal field from the black hole, which in turn affects the rotation of the star. The equations of motion for the orbit and the star's rotation can be written as

$$\ddot{f} + \frac{3}{2}\epsilon\frac{GM'}{a^3}\frac{I}{I_{\rm orb}}\sin\left[2(f-\theta)\right] = \dot{\Omega}_{\rm orb}\,, \tag{2}$$

$$\ddot{\theta} - \frac{3}{2}\epsilon\frac{GM'}{a^3}\sin\left[2(f-\theta)\right] = \dot{\Omega}_{\rm spin}\,, \tag{3}$$

where M' is the black hole mass, I and $I_{\rm orb}$ are the moments of inertia of the star and the orbit, respectively. f is the true anomaly and θ is the rotation angle of the neutron star, as shown in Fig. 1. $\dot{\Omega}_{\rm orb}$ is the orbital decay rate and $\dot{\Omega}_{\rm spin}$ is the neutron star spin down rate due to electromagnetic radiation, gravitational-wave radiation and the tidal dissipation. We set $\dot{\Omega}_{\rm spin}$ to zero, since it is negligible compared to $\dot{\Omega}_{\rm orb}$, within the regime of our interest. We also neglect the $I/I_{\rm orb}$ term in Eq. (2) since $I \ll I_{\rm orb}$. By defining the relative phase $\gamma = 2\theta - 2f$, and combining Eqs. (2) and (3) we obtain the following equation

$$\ddot{\gamma} + \mathcal{B}\sin\gamma + \mathcal{C} = 0\,, \tag{4}$$

where $\mathcal{B} = 3\epsilon GM'/a^3$ and $\mathcal{C} = 2\dot{\Omega}_{\rm orb}$.

Equation (4) resembles the equation of motion of a rigid pendulum that is subject to a periodic torque and a (nearly) constant external torque. Such systems generally exhibit two types of motion: circulation and libration. When $\mathcal{B} > \mathcal{C}$, resonance locking becomes possible, driving the system into a libration state in which the stellar spin and orbital frequency evolve synchronously. The general theory of resonance capture predicts that the probability of entering resonance is approximately [52–54]

$$\mathcal{P}_{\rm lock} = \frac{2}{1 + \frac{\pi}{2}\frac{\mathcal{B}^{1/2}\mathcal{C}}{\dot{\mathcal{B}}}} \approx \frac{4}{\pi}\frac{\dot{\mathcal{B}}}{\mathcal{B}^{1/2}\mathcal{C}} = \frac{4\sqrt{3}}{\pi}\left(\frac{q}{1+q}\right)^{1/2}\epsilon^{1/2}\,, \tag{5}$$

where we have used the relation $\dot{\Omega}_{\rm orb} = -\frac{3}{2}\frac{\dot{a}}{a}\Omega_{\rm orb}$ and $q = M'/M$ is the mass ratio. This is also confirmed by our numerical investigations.

On the other hand, when $\mathcal{B} < \mathcal{C}$, the resonance cannot be sustained and eventually breaks down. This occurs when the orbital frequency reaches a critical value, which we denote as $\Omega_{\rm br}$. At this point, the corresponding gravitational wave frequency is given by

$$\begin{aligned} f_{\rm br} &= \frac{\Omega_{\rm br}}{\pi} = \frac{1}{\pi(M+M')}\left(\frac{5}{64}\frac{M+M'}{M}\right)^{3/5}\epsilon^{3/5} \\ &\approx 10\left(\frac{1}{1+q}\right)^{2/5}\left(\frac{1.4\,M_\odot}{M}\right)\left(\frac{\epsilon}{10^{-5}}\right)^{3/5}\,\text{Hz}\,. \end{aligned} \tag{6}$$

In Fig. 2, we present an illustrative example of locking by numerically evolving Eqs. (2) and (3), where $M = 1.4\,M_\odot$, $q = 3$ and $\epsilon = 5\times10^{-5}$. The evolution starts with an initial orbital frequency of $f_{\rm orb} = 0.4\,$Hz and an initial neutron star spin frequency of $f_{\rm spin} = 0.5\,$Hz. As $f_{\rm orb}$ increases and passes through 0.5 Hz, resonance occurs and $f_{\rm spin}$ begins to evolve synchronously with $f_{\rm orb}$. This locking continues until $f_{\rm orb}$ reaches about 7.1 Hz (corresponding to $f_{\rm br} = 14.2\,$Hz), at which point the locking breaks down.

Resonance locking will induce the angular momentum exchange between the orbit and the neutron star, which should affect the orbital decay and cause a phase shift in the gravitational waveform. Using the formula $d^2\psi/d\omega^2 = 2(dE/d\omega)/\dot{E}$ for the phase $\psi(f)$ of the frequency domain waveform $\tilde{h}(f) = \mathcal{A}e^{i\psi(f)}$ [55], we derive the phase correction due to resonance locking as

$$\delta\psi_{\rm lock}(f) = \begin{cases} -\dfrac{45}{64}\dfrac{I}{\mu^2 M_t}\left(\dfrac{1}{v} - \dfrac{4}{3v_i} + \dfrac{v^3}{3v_i^4}\right), & f \le f_{br}\,, \\ -\dfrac{45}{64}\dfrac{I}{\mu^2 M_t}\left(\dfrac{1}{v_{\rm br}} - \dfrac{4}{3v_i} + \dfrac{v_{\rm br}^3}{3v_i^4}\right), & f > f_{br}\,. \end{cases} \tag{7}$$

where $M_t = M + M'$ and $\mu = MM'/M_t$ are the total mass and the reduced mass, respectively. Here $v = (\pi M_t f)^{1/3}$, $v_i < v_{\rm br}$ is an arbitrary constant related to the initial time and phase of the waveform. The correction clearly enters at 2PN (Post-Newtonian) order, with a large prefactor $\sim I/(\mu^2 M_t) \sim (R/M)^2$. For a NSBH system with $M = 1.4\,M_\odot$ and $M' \in [3\,M_\odot, 10\,M_\odot]$, the accumulated phase correction reaches $\mathcal{O}(1)$ radians when integrated from a start frequency of 5 Hz up to a breaking frequency $f_{\rm br} = 10\,$Hz.

INJECTION STUDIES

The large phase modulation suggests that resonance locking may be detectable, given sufficient detector sensitivity at low frequencies. To investigate the detection prospect, we perform injection studies to evaluate whether its signature can be reconstructed in parameter estimation for the upgrade of Advanced LIGO [56] (A+) and 3G detector network [57] (Cosmic Explorer [58–60] and Einstein Telescope [61–63]; CE+ET), based on their designed sensitivities. We consider two representative systems: a NSBH system with $q = 5$ ($M' = 5M = 7\,M_\odot$) and an equal-mass BNS ($M' = M = 1.4\,M_\odot$), both placed at a luminosity distance of $d_L = 100\,$Mpc and the sky location of GW170817 with R.A. = 3.446 and DEC. = −0.408 [64]. We also assume a nonspinning companion and an orientation with $\theta_{\rm JN} = 2.57$. Because the locked neutron star has a spin frequency below $f_{\rm br}$, we also neglect its spin in the waveform model. The TaylorF2 waveform [65], including tidal effects [66], is used as the baseline waveform for the BNS system, while IMRPhenomXPHM waveform [67] is employed for the NSBH system (tidal effects are not included, as they are marginally small in this case). We also adopt APR model [68] as fiducial EOS, which corresponds to a tidal deformability of $\Lambda = 248$ and a moment of inertia of $I = 30.18\,M_\odot^3$ for a $1.4\,M_\odot$ neutron star. For each merger, we calculate the expected SNR as $\rho = \sqrt{\sum_{{\rm det.}\,k}\langle h_k|h_k\rangle}$, where the inner product is defined as

$$\langle h_k|g_k\rangle = 2\int\frac{h_k^*(f)g_k(f) + h_k(f)g_k^*(f)}{S_{{\rm n},k}(f)}df\,, \tag{8}$$

where $S_{{\rm n},k}$ and h_k are the noise power spectrum density (PSD) and the signal strain of the k-th detector, respectively. For the NSBH system, the SNRs can reach 117 with A+ and 2135 with CE+ET, while for the BNS case, the corresponding SNRs are 69 and 1190. Owing to these high SNR values, we adopt the approach of injecting into zero-noise [69]. The parameter estimations are performed with Bilby [70], with injection and template waveforms all having a low-frequency cutoff of 5 Hz and ending when the system reaches $f_{\rm ISCO} = 1/(6^{3/2}\pi M_t)$, where $f_{\rm ISCO}$ is

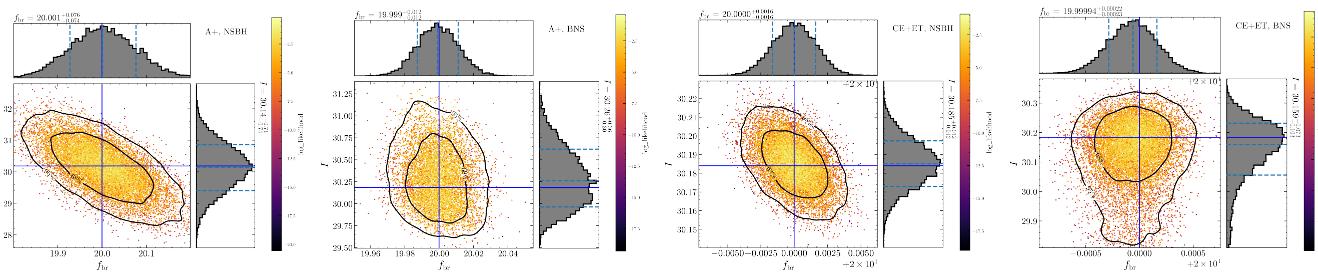

FIG. 3. Posterior distributions of breaking frequency $f_{\rm br}$ and moment of inertia I for different recovered injections. The injection values are marked with blue lines.

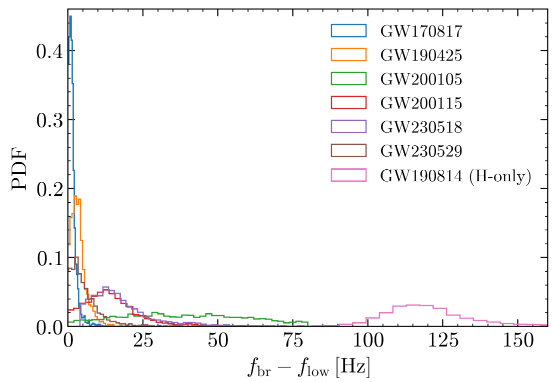

FIG. 4. Posterior distributions of breaking frequency $f_{\rm br}$ for the search in several GW events. Here, $f_{\rm low}$ indicates the minimum frequency of our search range. Note that the results for GW190814 shown in the figure are based on the Hanford data only.

the GW frequency at the innermost stable circular orbit (ISCO).

We first inject a locking signal with $f_{\rm br} = 20\,$Hz. In Fig. 3, we show the posterior distributions of $f_{\rm br}$ and I. We find that in all cases, the injected values can be well reconstructed. For A+, the measurement accuracies of $f_{\rm br}$ and I can reach 0.1% and 1%, respectively. For CE+ET, these accuracies can be further improved by up to an order of magnitude. We also inject locking signals with a lower breaking frequency of $f_{\rm br} = 10\,$Hz (see Supplemental Material [71]). In this case, although CE+ET is still able to reconstruct the injected parameters, A+ fails to do so. The reason is that the SNR accumulated in the $5-10\,$Hz band is only $\rho \sim \mathcal{O}(1)$ for A+, providing essentially no information, whereas CE+ET collects a SNR of $\rho \sim \mathcal{O}(100)$ in the same frequency band, enabling precise measurements.

SEARCHES

We further perform a signal search for all known GW events with NS. These include four NSBH systems (GW200105 and GW200115 [72], GW230518 [73], GW230529 [74]), two BNS systems (GW170817 [75] and GW190425 [76]) and one system with a $2.6\,M_\odot$ mass-gap object (GW190814 [77]). For this analysis, we have used publicly available GW strain data [78] and noise PSDs and followed an inference procedure similar to that conducted by LIGO [79], Virgo [80], and KAGRA [81] (LVK) collaboration. For BNS mergers, we adopt the TaylorF2 waveform as the baseline waveform, while for the NSBH mergers we employ the IMRPhenomNSBH waveform [82] except for GW200105. GW200105 has been reported with orbital eccentricity [28], and therefore our circular-orbit GW phase correction, Eq. (7), is not applicable in this case. Instead, we modify the equations of motion by incorporating the locking correction on top of the post-Newtonian inspiral-only waveform model (pyEFPE) developed in Ref. [83] (see the Supplemental Material [51] for details). We have validated that, in the limit of vanishing eccentricity, the waveform correction consistently reproduces the results obtained from our analytical formula for circular-orbit in Eq. (7). For GW190814, we adopt the IMRPhenomXPHM waveform [67], which incorporates higher-order multipoles, as the event exhibits strong evidence for them [77].

In Fig. 4, we show the posterior distributions of $f_{\rm br} - f_{\rm low}$ for the seven systems. Here, $f_{\rm low}$ indicates the minimum frequency of our search range, which is 23 Hz for GW170817 and 20 Hz for the other systems. It is obvious that no significant sign for $f_{\rm br} > f_{\rm low}$ is observed in both NSBH and BNS systems. In the hypotheses test framework, if we denote the absence of a locking signal as model $\mathcal{H}_0$ and the presence of a locking signal as model $\mathcal{H}_1$, the Savage–Dickey density ratio method [84] can be used to estimate the Bayes factors between them, i.e.,

$$\mathcal{B}_0^1 = \lim_{f_{\rm br}\to f_{\rm low}} \frac{p(f_{\rm br}|\mathcal{H}_1)}{p(f_{\rm br}|D,\mathcal{H}_1)} \tag{9}$$

where D refers to the observational data. For these four NSBH and two BNS systems, the resulting Bayes factors $\ln \mathcal{B}_0^1$ are in the range $[-3.4, -0.65]$, indicating that there is no preference for model $\mathcal{H}_1$ relative to model $\mathcal{H}_0$ [85].

In the case of GW190814, a separate peak at $f_{\rm br} \simeq 130\,$Hz is observed using the Hanford data. However,

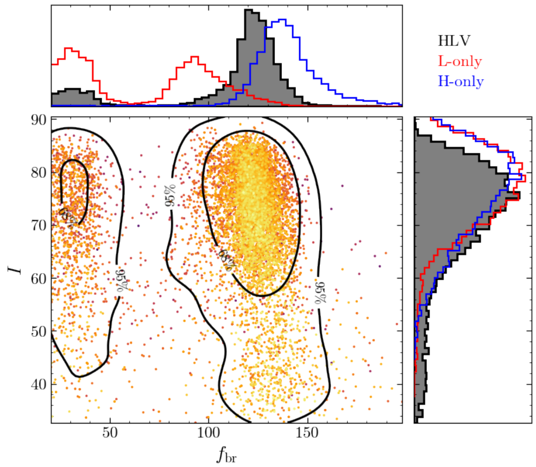

FIG. 5. Posterior distributions of breaking frequency $f_{\rm br}$ and moment of inertia I with Hanford-Livingston-Virgo data (black, grey shading), Livingston data only (red) and Hanford data only (blue), for GW190814.

when we only consider the Livingston data or combine the Hanford-Livingston-Virgo data, this peak weakens and a bimodal distribution for $f_{\rm br}$ emerges, as seen in Fig. 5. The left peak is consistent with the absence of a locking signal, while the right peak may correspond to a locking signal lasting until $f_{\rm br} \sim 120\,\mathrm{Hz}$. We are unable to determine which scenario is preferred. For Hanford-Livingston-Virgo data, the Bayes factor obtained remains inconclusive, with a value of $\ln \mathcal{B}_0^1 = 0.11$. It should be noted that LIGO Hanford was not in observing mode during the event, but its data is still usable [77]. Furthermore, thunderstorms near Livingston caused noise in the $\lesssim 30\,\mathrm{Hz}$ band, as reported in [77]. If the $f_{\rm br} \sim 120\,\mathrm{Hz}$ peak is real, it would imply that the secondary object of GW190814 is not a black hole, but rather a neutron star with an ellipticity of $\epsilon \sim 8 \times 10^{-3}$. This would correspond to an extremely strong internal magnetic field inside the neutron star, with $\bar{B} \sim 8 \times 10^{16}\,\mathrm{G}$ [taking $\kappa = 1$ in Eq. (1)].

DISCUSSION AND CONCLUSION

In this work, we present a novel resonance locking mechanism–the sustained spin-orbit resonance –that may occur in neutron-star binaries. Locking occurs when the orbital frequency sweeps through the neutron star spin frequency, typically occurring in the range of $0.1 - 1\,\mathrm{Hz}$ for magnetars, which lies within the frequency band of space-based detectors like DECIGO [86]. However, because of the relatively large ellipticity of magnetars, the locking can persist up to $\mathcal{O}(10)$Hz or higher, making it detectable by ground-based detectors such as A+ and CE+ET. Although we have not yet observed a positive event, further searches should be conducted to facilitate discovery or place meaningful constraints.

The expected merger rate for a resonance-locking NSBH system is approximately

$$\begin{aligned} \mathcal{R}_{\rm lock} &= f_{\rm mag} \mathcal{P}_{\rm lock} \mathcal{R}_{\rm NSBH} \\ &\approx 0.18\, f_{\rm mag} \left(\frac{\epsilon}{10^{-5}}\right)^{1/2} \left(\frac{\mathcal{R}_{\rm NSBH}}{30\,\mathrm{Gpc}^{-3}\,\mathrm{yr}^{-1}}\right) \mathrm{Gpc}^{-3}\,\mathrm{yr}^{-1}\,, \end{aligned} \tag{10}$$

where $f_{\rm mag}$ is the fraction of neutron stars that are magnetars in NSBH events. If we take a volumetric merger rate (number of mergers per comoving volume per cosmic time at redshift z) as $\mathcal{R}(z) = \mathcal{R}_{\rm lock} \times (1+z)^{3.2} e^{-z^2/3}$ for $z < 6$, then the total merger rate in the observer frame is written as

$$\begin{aligned} \dot{N} &= \int \frac{dV_c(z)}{dz} \frac{\mathcal{R}(z)}{1+z} dz \\ &= 603\, f_{\rm mag} \left(\frac{\epsilon}{10^{-5}}\right)^{1/2} \left(\frac{\mathcal{R}_{\rm NSBH}}{30\,\mathrm{Gpc}^{-3}\,\mathrm{yr}^{-1}}\right) \mathrm{yr}^{-1} \end{aligned} \tag{11}$$

where $V_c(z)$ is the comoving volume up to redshift z. However, not all resonance-locking signals in these merger events can be individually resolved by CE+ET. To quantify resolvable events, we generate a synthetic NSBH population of 10^5 mergers (see Supplemental Material [51]). We then place this population at different redshifts to evaluate the resolvable fraction, $f_{\rm res}(z)$. For each choice of ϵ, we evaluate the corresponding breaking frequency $f_{\rm br}$ for the population and identify mergers as resolvable if the accumulated SNR in the frequency band $[1\,\mathrm{Hz}, f_{\rm br}]$ exceeds the threshold $\rho_{\rm thr} = 10$. This allows us to estimate the resolvable merger events as

$$\dot{N}_{\rm res} = \int \frac{dV_c(z)}{dz} \frac{\mathcal{R}(z)}{1+z} f_{\rm res}(z) dz\,, \tag{12}$$

and hence the expected observing time for CE+ET to detect one positive event,

$$T_{\rm obs} = \frac{1}{\dot{N}_{\rm res}}\,. \tag{13}$$

In Fig. 6 we show $T_{\rm obs}$ as a function of $f_{\rm mag}$ and ϵ. We note that ET performs better than CE at low frequencies ($< 5\,\mathrm{Hz}$), so for relatively small values of ϵ ($\lesssim 10^{-5}$), the detection capability is determined primarily by ET.

However, successful detection of a resonance locking signal will bring in profound opportunities for studying neutron stars in terms of formation mechanism and fundamental physics tests. First, the measurement of $f_{\rm br}$ can be translated into neutron star ellipticity, which may provide direct evidence of a magnetar in the binary system. The measured ellipticity can further be used to infer the internal magnetic field strength. Second, such a detection enables the most precise measurement of the neutron star moment of inertia, with an accuracy that reaches 1% or even 0.1%, which offers powerful constraints on the

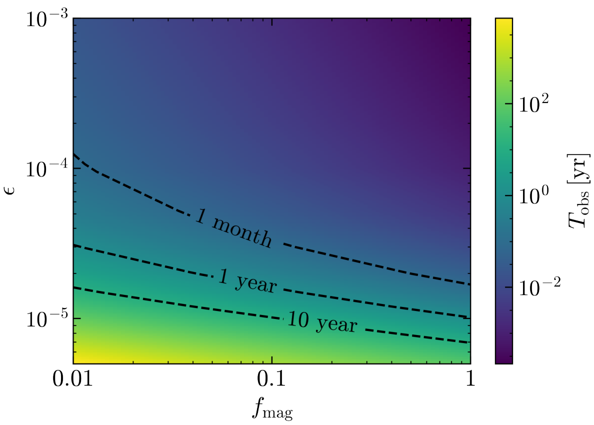

FIG. 6. The expected observing time for 3G detector network (CE+ET) to detect a positive event, as a function of the magnetar fraction f_{mag} in NSBH binaries and the ellipticity ϵ. We assume a rate of $\mathcal{R}_{\mathrm{NSBH}} = 30\,\mathrm{Gpc}^{-3}\,\mathrm{yr}^{-1}$ for NSBH mergers, which agrees with the current estimate $9.1 - 84\,\mathrm{Gpc}^{-3}\,\mathrm{yr}^{-1}$ from GW detections [87].

dense matter EOS [88, 89]. Note that currently the best method for measuring the neutron star moment of inertia is in the double pulsar system PSR J0737-3039 [90], where long-term pulsar timing is used to determine the periastron advance induced by the Lense-Thirring effect. This approach is expected to produce a measurement with $\sim 10\%$ precision by around 2030 [91]. Moreover, spin-orbit resonance locking systems allow simultaneous measurement of the moment of inertia and the tidal love number, providing a unique way to test gravity through the EOS-independent I-Love relation [92].

While our previous discussion has primarily focused on magnetars, which is the most astrophysically compelling explanation for neutron star ellipticity, the spin-orbit resonance locking mechanism is a general framework that can be applied to a wider range of scenarios. For example, systems involving elastic materials, such as neutron star crusts, solid-quark cores [93], or even solid-quark stars [94, 95], can sustain relatively large ellipticities. Theoretical estimates suggest that a solid crust can support a maximum ellipticity on the order of $\epsilon_{\max} \sim 10^{-6}(\sigma_{\mathrm{br}}/0.1)$ [96], with the breaking strain $\sigma_{\mathrm{br}} \sim 0.1$ from the molecular dynamics simulations of crustal fracture [97], while internal stress within a solid quark core or a solid quark star may allow even larger deformations. Moreover, exotic compact objects (ECO) have been proposed to deviate from Kerr black holes by supporting finite asymmetric deformations [98–100]. The resonance locking framework can be applied to test these black hole mimickers and to probe their deviations from Kerr geometry.

ACKNOWLEDGMENTS

We thank Yi-Fan Wang for the help with gravitational-wave data processing and parameter inference and Yong Gao for helpful discussion regarding the precession dynamics of triaxially-deformed neutron stars. Z.-Q. M. is supported by the Postdoctoral Innovation Talent Support Program of CPSF (No. BX20240223) and the China Postdoctoral Science Foundation funded project (No. 2024M761948). H. Y. is supported by the Natural Science Foundation of China (Grant 12573048).

This research has made use of data or software obtained from the Gravitational Wave Open Science Center (gwosc.org), a service of the LIGO Scientific Collaboration, the Virgo Collaboration, and KAGRA. This material is based upon work supported by NSF's LIGO Laboratory which is a major facility fully funded by the National Science Foundation, as well as the Science and Technology Facilities Council (STFC) of the United Kingdom, the Max-Planck-Society (MPS), and the State of Niedersachsen/Germany for support of the construction of Advanced LIGO and construction and operation of the GEO600 detector. Additional support for Advanced LIGO was provided by the Australian Research Council. Virgo is funded, through the European Gravitational Observatory (EGO), by the French Centre National de Recherche Scientifique (CNRS), the Italian Istituto Nazionale di Fisica Nucleare (INFN) and the Dutch Nikhef, with contributions by institutions from Belgium, Germany, Greece, Hungary, Ireland, Japan, Monaco, Poland, Portugal, Spain. KAGRA is supported by Ministry of Education, Culture, Sports, Science and Technology (MEXT), Japan Society for the Promotion of Science (JSPS) in Japan; National Research Foundation (NRF) and Ministry of Science and ICT (MSIT) in Korea; Academia Sinica (AS) and National Science and Technology Council (NSTC) in Taiwan.

* hyangdoa@tsinghua.edu.cn

[1] B. P. Abbott *et al.* (LIGO Scientific, Virgo), Observation of Gravitational Waves from a Binary Black Hole Merger, Phys. Rev. Lett. **116**, 061102 (2016), arXiv:1602.03837 [gr-qc].

[2] A. G. Abac *et al.* (KAGRA, Virgo, LIGO Scientific), GW250114: Testing Hawking's Area Law and the Kerr Nature of Black Holes, Phys. Rev. Lett. **135**, 111403 (2025), arXiv:2509.08054 [gr-qc].

[3] D. Lai, Resonant oscillations and tidal heating in coalescing binary neutron stars, Mon. Not. Roy. Astron. Soc. **270**, 611 (1994), arXiv:astro-ph/9404062.

[4] J. D. Schnittman, Spin-orbit resonance and the evolution of compact binary systems, Phys. Rev. D **70**, 124020 (2004), arXiv:astro-ph/0409174.

[5] Z. Pan, Z. Lyu, B. Bonga, N. Ortiz, and H. Yang, Probing Crust Meltdown in Inspiraling Binary Neu-

tron Stars, Phys. Rev. Lett. **125**, 201102 (2020), arXiv:2003.03330 [astro-ph.HE].
[6] E. Poisson, Gravitomagnetic tidal resonance in neutron-star binary inspirals, Phys. Rev. D **101**, 104028 (2020), arXiv:2003.10427 [gr-qc].
[7] K. J. Kwon, H. Yu, and T. Venumadhav, Resonance Locking of Anharmonic g-Modes in Coalescing Neutron Star Binaries, arXiv e-prints , arXiv:2410.03831 (2024), arXiv:2410.03831.
[8] D. Gerosa, R. O'Shaughnessy, M. Kesden, E. Berti, and U. Sperhake, Distinguishing black-hole spin-orbit resonances by their gravitational-wave signatures, Phys. Rev. D **89**, 124025 (2014), arXiv:1403.7147 [gr-qc].
[9] Z. Miao, X. Feng, Z. Pan, and H. Yang, Relativistic excitation of compact stars, arXiv e-prints , arXiv:2506.23176 (2025), arXiv:2506.23176 [gr-qc].
[10] L. London, D. Shoemaker, and J. Healy, Modeling ringdown: Beyond the fundamental quasinormal modes, Phys. Rev. D **90**, 124032 (2014), [Erratum: Phys.Rev.D 94, 069902 (2016)], arXiv:1404.3197 [gr-qc].
[11] M. H.-Y. Cheung *et al.*, Nonlinear Effects in Black Hole Ringdown, Phys. Rev. Lett. **130**, 081401 (2023), arXiv:2208.07374 [gr-qc].
[12] K. Mitman *et al.*, Nonlinearities in Black Hole Ringdowns, Phys. Rev. Lett. **130**, 081402 (2023), arXiv:2208.07380 [gr-qc].
[13] M. H.-Y. Cheung, E. Berti, V. Baibhav, and R. Cotesta, Extracting linear and nonlinear quasinormal modes from black hole merger simulations, Phys. Rev. D **109**, 044069 (2024), [Erratum: Phys.Rev.D 110, 049902 (2024), Erratum: Phys.Rev.D 112, 049901 (2025)], arXiv:2310.04489 [gr-qc].
[14] N. Khera, A. Ribes Metidieri, B. Bonga, X. Jiménez Forteza, B. Krishnan, E. Poisson, D. Pook-Kolb, E. Schnetter, and H. Yang, Nonlinear Ringdown at the Black Hole Horizon, Phys. Rev. Lett. **131**, 231401 (2023), arXiv:2306.11142 [gr-qc].
[15] T. May, S. Ma, J. L. Ripley, and W. E. East, Nonlinear effect of absorption on the ringdown of a spinning black hole, Phys. Rev. D **110**, 084034 (2024), arXiv:2405.18303 [gr-qc].
[16] N. Khera, S. Ma, and H. Yang, Quadratic Mode Couplings in Rotating Black Holes and Their Detectability, Phys. Rev. Lett. **134**, 211404 (2025), arXiv:2410.14529 [gr-qc].
[17] S. Ma and H. Yang, Excitation of quadratic quasinormal modes for Kerr black holes, Phys. Rev. D **109**, 104070 (2024), arXiv:2401.15516 [gr-qc].
[18] Y. B. Zel'dovich and A. G. Polnarev, Radiation of gravitational waves by a cluster of superdense stars, Sov. Astron. **18**, 17 (1974).
[19] D. Christodoulou, Nonlinear nature of gravitation and gravitational wave experiments, Phys. Rev. Lett. **67**, 1486 (1991).
[20] M. Favata, Post-Newtonian corrections to the gravitational-wave memory for quasi-circular, inspiralling compact binaries, Phys. Rev. D **80**, 024002 (2009), arXiv:0812.0069 [gr-qc].
[21] M. Favata, Nonlinear gravitational-wave memory from binary black hole mergers, Astrophys. J. Lett. **696**, L159 (2009), arXiv:0902.3660 [astro-ph.SR].
[22] P. D. Lasky, E. Thrane, Y. Levin, J. Blackman, and Y. Chen, Detecting gravitational-wave memory with LIGO: implications of GW150914, Phys. Rev. Lett. **117**, 061102 (2016), arXiv:1605.01415 [astro-ph.HE].
[23] A. Strominger and A. Zhiboedov, Gravitational Memory, BMS Supertranslations and Soft Theorems, JHEP **01**, 086, arXiv:1411.5745 [hep-th].
[24] H. Yang and D. Martynov, Testing Gravitational Memory Generation with Compact Binary Mergers, Phys. Rev. Lett. **121**, 071102 (2018), arXiv:1803.02429 [gr-qc].
[25] R. Abbott *et al.* (LIGO Scientific, VIRGO, KAGRA, Virgo), Searches for Continuous Gravitational Waves from Young Supernova Remnants in the Early Third Observing Run of Advanced LIGO and Virgo, Astrophys. J. **921**, 80 (2021), arXiv:2105.11641 [astro-ph.HE].
[26] R. Abbott *et al.* (LIGO Scientific, VIRGO, KAGRA), Search for continuous gravitational waves from 20 accreting millisecond x-ray pulsars in O3 LIGO data, Phys. Rev. D **105**, 022002 (2022), arXiv:2109.09255 [astro-ph.HE].
[27] N. Loutrel, R. Brito, A. Maselli, and P. Pani, Inspiraling compact objects with generic deformations, Phys. Rev. D **105**, 124050 (2022), arXiv:2203.01725 [gr-qc].
[28] G. Morras, G. Pratten, and P. Schmidt, Orbital eccentricity in a neutron star - black hole binary, arXiv e-prints , arXiv:2503.15393 (2025), arXiv:2503.15393 [astro-ph.HE].
[29] K. Kacanja, K. Soni, and A. H. Nitz, Eccentricity signatures in LIGO-Virgo-KAGRA's BNS and NSBH binaries, arXiv e-prints , arXiv:2508.00179 (2025), arXiv:2508.00179 [gr-qc].
[30] A. Jan, B.-J. Tsao, R. O'Shaughnessy, D. Shoemaker, and P. Laguna, GW200105: A detailed study of eccentricity in the neutron star-black hole binary, arXiv e-prints , arXiv:2508.12460 (2025), arXiv:2508.12460 [gr-qc].
[31] J. Stegmann and J. Klencki, Spin-orbit misalignment and residual eccentricity are evidence that neutron star-black hole mergers form through triple star evolution, arXiv e-prints , arXiv:2506.09121 (2025), arXiv:2506.09121 [astro-ph.HE].
[32] J. Samsing, M. MacLeod, and E. Ramirez-Ruiz, The Formation of Eccentric Compact Binary Inspirals and the Role of Gravitational Wave Emission in Binary-Single Stellar Encounters, Astrophys. J. **784**, 71 (2014), arXiv:1308.2964 [astro-ph.HE].
[33] D. Clausen, S. Sigurdsson, and D. F. Chernoff, Black Hole-Neutron Star Mergers in Globular Clusters, Mon. Not. Roy. Astron. Soc. **428**, 3618 (2013), arXiv:1210.8153 [astro-ph.HE].
[34] W. H. Lee, E. Ramirez-Ruiz, and G. van de Ven, Short gamma-ray bursts from dynamically-assembled compact binaries in globular clusters: pathways, rates, hydrodynamics and cosmological setting, Astrophys. J. **720**, 953 (2010), arXiv:0909.2884 [astro-ph.HE].
[35] B. Kocsis and J. Levin, Repeated Bursts from Relativistic Scattering of Compact Objects in Galactic Nuclei, Phys. Rev. D **85**, 123005 (2012), arXiv:1109.4170 [astro-ph.CO].
[36] C. Petrovich and F. Antonini, Greatly enhanced merger rates of compact-object binaries in non-spherical nuclear star clusters, Astrophys. J. **846**, 146 (2017), arXiv:1705.05848 [astro-ph.HE].
[37] L. Wen, On the eccentricity distribution of coalescing black hole binaries driven by the Kozai mecha-

nism in globular clusters, Astrophys. J. **598**, 419 (2003), arXiv:astro-ph/0211492.

[38] B. Liu and D. Lai, Black Hole and Neutron Star Binary Mergers in Triple Systems: Merger Fraction and Spin–Orbit Misalignment, Astrophys. J. **863**, 68 (2018), arXiv:1805.03202 [astro-ph.HE].

[39] H. V. Zeipel, Sur l'application des séries de m. lindstedt à l'étude du mouvement des comètes périodiques, Astronomische Nachrichten **183**, 345 (1909), https://onlinelibrary.wiley.com/doi/pdf/10.1002/asna.19091832202.

[40] M. L. Lidov, The evolution of orbits of artificial satellites of planets under the action of gravitational perturbations of external bodies, Planetary and Space Science **9**, 719 (1962).

[41] Y. Kozai, Secular perturbations of asteroids with high inclination and eccentricity, AJ **67**, 591 (1962).

[42] P. Goldreich and A. Reisenegger, Magnetic Field Decay in Isolated Neutron Stars, Astrophys. J. **395**, 250 (1992).

[43] Recently, a Fast Radio Burst (FRB) was reported to be located in a globular cluster [**?**]. If this FRB is linked to a magnetar, it could imply that the activate lifetime of magnetars might be longer than previously thought [**?**].

[44] R. Gill and J. Heyl, The Birthrate of Magnetars, Mon. Not. Roy. Astron. Soc. **381**, 52 (2007), arXiv:astro-ph/0703346.

[45] M. Gullón, J. A. Pons, J. A. Miralles, D. Viganò, N. Rea, and R. Perna, Population synthesis of isolated neutron stars with magneto-rotational evolution – II. From radio-pulsars to magnetars, Mon. Not. Roy. Astron. Soc. **454**, 615 (2015), arXiv:1507.05452 [astro-ph.HE].

[46] P. Beniamini, K. Hotokezaka, A. van der Horst, and C. Kouveliotou, Formation Rates and Evolution Histories of Magnetars, Mon. Not. Roy. Astron. Soc. **487**, 1426 (2019), arXiv:1903.06718 [astro-ph.HE].

[47] Y. Gao, L. Shao, G. Desvignes, D. I. Jones, M. Kramer, and G. Yim, Precession of magnetars: dynamical evolutions and modulations on polarized electromagnetic waves, Mon. Not. Roy. Astron. Soc. **519**, 1080 (2023), arXiv:2211.17087 [astro-ph.HE].

[48] B. Haskell, L. Samuelsson, K. Glampedakis, and N. Andersson, Modelling magnetically deformed neutron stars, Mon. Not. Roy. Astron. Soc. **385**, 531 (2008), arXiv:0705.1780 [astro-ph].

[49] A. Mastrano, A. Melatos, A. Reisenegger, and T. Akgun, Gravitational wave emission from a magnetically deformed non-barotropic neutron star, Mon. Not. Roy. Astron. Soc. **417**, 2288 (2011), arXiv:1108.0219 [astro-ph.HE].

[50] A. Mastrano, A. G. Suvorov, and A. Melatos, Neutron star deformation due to poloidal-toroidal magnetic fields of arbitrary multipole order: a new analytic approach, Mon. Not. Roy. Astron. Soc. **447**, 3475 (2015), arXiv:1501.01134 [astro-ph.HE].

[51] See Supplemental Material at [URL will be inserted by publisher] for additional figures, derivations, and experimental details.

[52] C. F. Yoder, Diagrammatic Theory of Transition of Pendulum-like Systems, Celestial Mechanics **19**, 3 (1979).

[53] J. Henrard, Capture Into Resonance - an Extension of the Use of Adiabatic Invariants, Celestial Mechanics **27**, 3 (1982).

[54] C. D. Murray and S. F. Dermott, *Solar System Dynamics* (Cambridge University Press, 2000).

[55] W. Tichy, E. E. Flanagan, and E. Poisson, Can the postNewtonian gravitational wave form of an inspiraling binary be improved by solving the energy balance equation numerically?, Phys. Rev. D **61**, 104015 (2000), arXiv:gr-qc/9912075.

[56] L. Barsotti, L. McCuller, M. Evans, and P. Fritschel, The A+ design curve, `https://dcc.ligo.org/LIGO-T1800042/public` (2018).

[57] B. P. Abbott *et al.* (KAGRA, LIGO Scientific, Virgo), Prospects for observing and localizing gravitational-wave transients with Advanced LIGO, Advanced Virgo and KAGRA, Living Rev. Rel. **19**, 1 (2016), arXiv:1304.0670 [gr-qc].

[58] B. P. Abbott *et al.* (LIGO Scientific), Exploring the Sensitivity of Next Generation Gravitational Wave Detectors, Class. Quant. Grav. **34**, 044001 (2017), arXiv:1607.08697 [astro-ph.IM].

[59] D. Reitze *et al.*, Cosmic Explorer: The U.S. Contribution to Gravitational-Wave Astronomy beyond LIGO, Bull. Am. Astron. Soc. **51**, 035 (2019), arXiv:1907.04833 [astro-ph.IM].

[60] M. Evans, R. X. Adhikari, C. Afle, S. W. Ballmer, S. Biscoveanu, S. Borhanian, D. A. Brown, Y. Chen, R. Eisenstein, A. Gruson, A. Gupta, E. D. Hall, R. Huxford, B. Kamai, R. Kashyap, J. S. Kissel, K. Kuns, P. Landry, A. Lenon, G. Lovelace, L. McCuller, K. K. Y. Ng, A. H. Nitz, J. Read, B. S. Sathyaprakash, D. H. Shoemaker, B. J. J. Slagmolen, J. R. Smith, V. Srivastava, L. Sun, S. Vitale, and R. Weiss, A Horizon Study for Cosmic Explorer: Science, Observatories, and Community, arXiv e-prints , arXiv:2109.09882 (2021), arXiv:2109.09882 [astro-ph.IM].

[61] M. Punturo *et al.*, The third generation of gravitational wave observatories and their science reach, Class. Quant. Grav. **27**, 084007 (2010).

[62] S. Hild *et al.*, Sensitivity Studies for Third-Generation Gravitational Wave Observatories, Class. Quant. Grav. **28**, 094013 (2011), arXiv:1012.0908 [gr-qc].

[63] The ET science team, Einstein gravitational wave telescope (et) conceptual design study, `https://apps.et-gw.eu/tds/?r=8709` (2011).

[64] B. P. Abbott *et al.*, Multi-messenger Observations of a Binary Neutron Star Merger, Astrophys. J. Lett. **848**, L12 (2017), arXiv:1710.05833 [astro-ph.HE].

[65] A. Buonanno, B. Iyer, E. Ochsner, Y. Pan, and B. S. Sathyaprakash, Comparison of post-Newtonian templates for compact binary inspiral signals in gravitational-wave detectors, Phys. Rev. D **80**, 084043 (2009), arXiv:0907.0700 [gr-qc].

[66] J. Vines, E. E. Flanagan, and T. Hinderer, Post-1-Newtonian tidal effects in the gravitational waveform from binary inspirals, Phys. Rev. D **83**, 084051 (2011), arXiv:1101.1673 [gr-qc].

[67] G. Pratten *et al.*, Computationally efficient models for the dominant and subdominant harmonic modes of precessing binary black holes, Phys. Rev. D **103**, 104056 (2021), arXiv:2004.06503 [gr-qc].

[68] A. Akmal, V. R. Pandharipande, and D. G. Ravenhall, The Equation of state of nucleon matter and neutron star structure, Phys. Rev. C **58**, 1804 (1998), arXiv:nucl-th/9804027.

[69] C. L. Rodriguez, B. Farr, V. Raymond, W. M. Farr, T. B. Littenberg, D. Fazi, and V. Kalogera, Basic Parameter Estimation of Binary Neutron Star Systems by the Advanced LIGO/Virgo Network, Astrophys. J. **784**, 119 (2014), arXiv:1309.3273 [astro-ph.HE].

[70] G. Ashton *et al.*, BILBY: A user-friendly Bayesian inference library for gravitational-wave astronomy, Astrophys. J. Suppl. **241**, 27 (2019), arXiv:1811.02042 [astro-ph.IM].

[71] See Supplemental Material at [].

[72] R. Abbott *et al.* (LIGO Scientific, KAGRA, VIRGO), Observation of Gravitational Waves from Two Neutron Star–Black Hole Coalescences, Astrophys. J. Lett. **915**, L5 (2021), arXiv:2106.15163 [astro-ph.HE].

[73] A. G. Abac *et al.* (LIGO Scientific, VIRGO, KAGRA), GWTC-4.0: Updating the Gravitational-Wave Transient Catalog with Observations from the First Part of the Fourth LIGO-Virgo-KAGRA Observing Run, arXiv e-prints , arXiv:2508.18082 (2025), arXiv:2508.18082 [gr-qc].

[74] A. G. Abac *et al.* (LIGO Scientific, KAGRA, VIRGO), Observation of Gravitational Waves from the Coalescence of a 2.5–4.5 M $_\odot$ Compact Object and a Neutron Star, Astrophys. J. Lett. **970**, L34 (2024), arXiv:2404.04248 [astro-ph.HE].

[75] B. P. Abbott *et al.* (LIGO Scientific, Virgo), GW170817: Observation of Gravitational Waves from a Binary Neutron Star Inspiral, Phys. Rev. Lett. **119**, 161101 (2017), arXiv:1710.05832 [gr-qc].

[76] B. P. Abbott *et al.* (LIGO Scientific, Virgo), GW190425: Observation of a Compact Binary Coalescence with Total Mass $\sim 3.4 M_\odot$, Astrophys. J. Lett. **892**, L3 (2020), arXiv:2001.01761 [astro-ph.HE].

[77] R. Abbott *et al.* (LIGO Scientific, Virgo), GW190814: Gravitational Waves from the Coalescence of a 23 Solar Mass Black Hole with a 2.6 Solar Mass Compact Object, Astrophys. J. Lett. **896**, L44 (2020), arXiv:2006.12611 [astro-ph.HE].

[78] A. G. Abac *et al.* (LIGO Scientific, VIRGO, KAGRA), Open Data from LIGO, Virgo, and KAGRA through the First Part of the Fourth Observing Run, arXiv e-prints , arXiv:2508.18079 (2025), arXiv:2508.18079 [gr-qc].

[79] J. Aasi *et al.* (LIGO Scientific), Advanced LIGO, Class. Quant. Grav. **32**, 074001 (2015), arXiv:1411.4547 [gr-qc].

[80] F. Acernese *et al.* (VIRGO), Advanced Virgo: a second-generation interferometric gravitational wave detector, Class. Quant. Grav. **32**, 024001 (2015), arXiv:1408.3978 [gr-qc].

[81] T. Akutsu *et al.* (KAGRA), Overview of KAGRA: Detector design and construction history, PTEP **2021**, 05A101 (2021), arXiv:2005.05574 [physics.ins-det].

[82] J. E. Thompson, E. Fauchon-Jones, S. Khan, E. Nitoglia, F. Pannarale, T. Dietrich, and M. Hannam, Modeling the gravitational wave signature of neutron star black hole coalescences, Phys. Rev. D **101**, 124059 (2020), arXiv:2002.08383 [gr-qc].

[83] G. Morras, G. Pratten, and P. Schmidt, Improved post-Newtonian waveform model for inspiralling precessing-eccentric compact binaries, Phys. Rev. D **111**, 084052 (2025), arXiv:2502.03929 [gr-qc].

[84] J. M. Dickey, The weighted likelihood ratio, linear hypotheses on normal location parameters, The Annals of Mathematical Statistics **42**, 204 (1971).

[85] R. E. Kass and A. E. Raftery, Bayes factors, Journal of the American Statistical Association **90**, 773 (1995).

[86] S. Kawamura *et al.*, The Japanese space gravitational wave antenna: DECIGO, Class. Quant. Grav. **28**, 094011 (2011).

[87] A. G. Abac *et al.* (LIGO Scientific, VIRGO, KAGRA), GWTC-4.0: Population Properties of Merging Compact Binaries, arXiv e-prints , arXiv:2508.18083 (2025), arXiv:2508.18083 [astro-ph.HE].

[88] J. M. Lattimer and M. Prakash, Neutron star structure and the equation of state, Astrophys. J. **550**, 426 (2001), arXiv:astro-ph/0002232.

[89] Z. Miao, A. Li, and Z.-G. Dai, On the moment of inertia of PSR J0737-3039 A from LIGO/Virgo and NICER, Mon. Not. Roy. Astron. Soc. **515**, 5071 (2022), arXiv:2107.07979 [astro-ph.HE].

[90] M. Burgay *et al.*, An Increased estimate of the merger rate of double neutron stars from observations of a highly relativistic system, Nature **426**, 531 (2003), arXiv:astro-ph/0312071.

[91] H. Hu, M. Kramer, N. Wex, D. J. Champion, and M. S. Kehl, Constraining the dense matter equation-of-state with radio pulsars, Mon. Not. Roy. Astron. Soc. **497**, 3118 (2020), arXiv:2007.07725 [astro-ph.SR].

[92] K. Yagi and N. Yunes, I-Love-Q Relations in Neutron Stars and their Applications to Astrophysics, Gravitational Waves and Fundamental Physics, Phys. Rev. D **88**, 023009 (2013), arXiv:1303.1528 [gr-qc].

[93] M. G. Alford, J. A. Bowers, and K. Rajagopal, Crystalline color superconductivity, Phys. Rev. D **63**, 074016 (2001), arXiv:hep-ph/0008208.

[94] R.-X. Xu, Solid quark matter?, Astrophys. J. Lett. **596**, L59 (2003), arXiv:astro-ph/0302165.

[95] Z. Miao, C.-J. Xia, X.-Y. Lai, T. Maruyama, R.-X. Xu, and E.-P. Zhou, A bag model of matter condensed by the strong interaction, Int. J. Mod. Phys. E **31**, 2250037 (2022), arXiv:2008.06932 [nucl-th].

[96] G. Ushomirsky, C. Cutler, and L. Bildsten, Deformations of accreting neutron star crusts and gravitational wave emission, Mon. Not. Roy. Astron. Soc. **319**, 902 (2000), arXiv:astro-ph/0001136.

[97] C. J. Horowitz and K. Kadau, The Breaking Strain of Neutron Star Crust and Gravitational Waves, Phys. Rev. Lett. **102**, 191102 (2009), arXiv:0904.1986 [astro-ph.SR].

[98] G. Raposo, P. Pani, and R. Emparan, Exotic compact objects with soft hair, Phys. Rev. D **99**, 104050 (2019), arXiv:1812.07615 [gr-qc].

[99] M. Bianchi, D. Consoli, A. Grillo, J. F. Morales, P. Pani, and G. Raposo, Distinguishing fuzzballs from black holes through their multipolar structure, Phys. Rev. Lett. **125**, 221601 (2020), arXiv:2007.01743 [hep-th].

[100] C. A. R. Herdeiro, J. Kunz, I. Perapechka, E. Radu, and Y. Shnir, Multipolar boson stars: macroscopic Bose-Einstein condensates akin to hydrogen orbitals, Phys. Lett. B **812**, 136027 (2021), arXiv:2008.10608 [gr-qc].

[101] W. M. Kaula, Tests and combination of satellite determinations of the gravity field with gravimetry, Journal of Geophysical Research (1896-1977) **71**, 5303 (1966), https://agupubs.onlinelibrary.wiley.com/doi/pdf/10.1029/JZ071i022

[102] P. C. Peters, Gravitational Radiation and the Motion of Two Point Masses, Phys. Rev. **136**, B1224 (1964).

[103] A. C. M. Correia and J. Laskar, Long-term evolution of the spin of Mercury I. Effect of the obliquity and core-

mantle friction, Icarus **205**, 338 (2010), arXiv:0908.3912 [astro-ph.EP].

[104] N. Aghanim *et al.* (Planck), Planck 2018 results. VI. Cosmological parameters, Astron. Astrophys. **641**, A6 (2020), [Erratum: Astron.Astrophys. 652, C4 (2021)], arXiv:1807.06209 [astro-ph.CO].

Supplemental Material

ECCENETRIC ORBIT

In the main text, we discuss spin-orbit resonance locking for circular orbits. In this section, we extend the analysis to eccentric orbits. For simplicity, we still consider the case where the long axis of the neutron star lies within the orbital plane. In the next section, we will briefly discuss the more general scenario, where the long axis is oriented off the orbital plane.

Equation of Motion and the Probability of Capturing Resonance

The eccentric orbit can be described by

$$r = a(1 - e\cos u)\,, \tag{S14}$$

$$f = 2\arctan\left[\left(\frac{1+e}{1-e}\right)^{1/2}\tan\frac{u}{2}\right]\,, \tag{S15}$$

$$\ell \equiv n(t - t_0) = u - e\sin u\,, \tag{S16}$$

where a is the semi-major axis and e is the eccentricity. $n = \sqrt{G(M+M')/a^3}$ is the mean motion. The auxiliary variables u, f and ℓ are the eccentric, true and mean anomalies, respectively. t_0 is a constant of integration. With these notations, we can rewrite Eqs. (2) and (3) in the main text as

$$\ddot{\ell} = \dot{n}\,, \tag{S17}$$

$$\ddot{\theta} - \frac{3}{2}\epsilon n^2 \frac{q}{1+q}\frac{a^3}{r^3}\sin\left[2(f-\theta)\right] = 0\,, \tag{S18}$$

where we again omit the $I/I_{\rm orb}$ term and $\dot{\Omega}_{\rm spin}$ as done in the main text. Redefining $\gamma = 2\theta - 2p\ell$, we get

$$\ddot{\gamma} + 3\epsilon n^2 \frac{q}{1+q}\frac{a^3}{r^3}\sin(\gamma + 2p\ell - 2f) = -2p\dot{n}\,, \tag{S19}$$

By averaging all the terms in Eq. (S19) over one orbital period and expanding in terms of e, we then obtain [54]

$$\ddot{\gamma} + 3\epsilon n^2 \frac{q}{1+q} H(p,e)\sin\gamma = -2p\dot{n}\,, \tag{S20}$$

where $H(p,e) = G_{20(2p-2)}(e)$ with $G_{lpq}(e)$ the Kaula eccentricity function [101]. Only values of p that are integer multiples of $\frac{1}{2}$ will make $H(p,e)$ nonzero. For example,

$$H(1,e) = 1 - \frac{5}{2}e^2 + \frac{13}{16}e^4\,, \tag{S21}$$

$$H(\frac{3}{2},e) = \frac{7}{2}e - \frac{123}{116}e^3\,, \tag{S22}$$

$$H(2,e) = \frac{17}{2}e^2 - \frac{115}{6}e^4\,, \tag{S23}$$

$$H(\frac{5}{2},e) = \frac{845}{48}e^3\,. \tag{S24}$$

We rewrite Eq. (S20) as

$$\ddot{\gamma} + \mathcal{B}\sin\gamma + \mathcal{C} = 0\,, \tag{S25}$$

with

$$\mathcal{B} = 3\epsilon n^2 \frac{q}{1+q} H(p,e)\,, \tag{S26}$$

$$\mathcal{C} = 2p\dot{n}\,. \tag{S27}$$

According to the general theory of resonance capture [53], as $B_1 = -2\pi\mathcal{C} - 4\dot{\mathcal{B}}\mathcal{B}^{-1/2}$ is always negative for the neutron-star binaries in the inspiral phase, resonance can only occur if $B_1 + B_2 = -8\dot{\mathcal{B}}\mathcal{B}^{-1/2} < 0$ (B_1 and B_2 are the two balance of energy defined in Ref. [53]). This condition requires $\dot{\mathcal{B}} > 0$, which holds only for the $p = 1$ and $p = 3/2$ cases. *Therefore, for eccentric neutron-star binaries, spin-orbit resonance locking can only occur in the 1:1 and 3:2 modes.* The probability of capturing into resonance is then given by

$$\mathcal{P}(p,e) = \frac{2}{1 + \frac{\pi}{2}\frac{\mathcal{B}^{1/2}\mathcal{C}}{\dot{\mathcal{B}}}} \approx \frac{4}{\pi}\frac{\dot{\mathcal{B}}}{\mathcal{B}^{1/2}\mathcal{C}}$$
$$= \frac{4\sqrt{3}}{\pi p}\left(\frac{q}{1+q}\right)^{1/2}\epsilon^{1/2}\left(\sqrt{H(p,e)} + \frac{\dot{H}(p,e)}{2\sqrt{H(p,e)}}\frac{n}{\dot{n}}\right)\,. \tag{S28}$$

Substituting the evolution for the semi-major axis a and eccentricity e [102],

$$\dot{a} = -\frac{64}{5}\frac{MM'(M+M')}{a^3}\frac{1}{(1-e^2)^{7/2}}\left(1 + \frac{73}{24}e^2 + \frac{37}{96}e^4\right)\,, \tag{S29}$$

$$\dot{e} = -\frac{304}{15}\frac{MM'(M+M')}{a^4}\frac{e}{(1-e^2)^{5/2}}\left(1 + \frac{121}{304}e^2\right)\,, \tag{S30}$$

we obtain,

$$\mathcal{P}(1,e) = \frac{4\sqrt{3}}{\pi}\left(\frac{q}{1+q}\right)^{1/2}\epsilon^{1/2}\left(1 + \frac{25}{18}e^2\right)\,, \tag{S31}$$

$$\mathcal{P}(\frac{3}{2},e) = \frac{4\sqrt{3}}{\pi}\left(\frac{q}{1+q}\right)^{1/2}\epsilon^{1/2}\frac{17}{54}\sqrt{\frac{7}{2}}e^{1/2}\,. \tag{S32}$$

Gravitational waveform correction

In the main text, we derive the gravitational-wave phase correction due to resonance locking for circular orbits, which is not applicable to eccentric orbits. Here, we provide an alternative correction for eccentric orbits, based on the post-Newtonian inspiral-only waveform model (pyEFPE) developed in Ref. [83]. The equations of motion for y $[(1-e^2)y^2 = (M_t\omega)^{2/3}$ with $M_t = M + M'$

the total mass and ω the mean orbital angular velocity] and e^2 in Ref. [83] are given by

$$\mathcal{D}y = \nu y^9 \left(a_0 + \sum_{n=2}^{6} a_n y^n \right) , \tag{S33}$$

$$\mathcal{D}e^2 = -\nu y^8 \left(b_0 + \sum_{n=2}^{6} b_n y^n \right) , \tag{S34}$$

where $\nu = \mu/M_t$ is the symmetric mass ratio with the reduced mass $\mu = MM'/M_t$. a_n and b_n are PN coefficients with

$$a_0 = \frac{32}{5} + \frac{28}{5} e^2 \,, \tag{S35}$$

$$b_0 = \frac{608}{15} e^2 + \frac{242}{15} e^4 \,, \tag{S36}$$

and $\mathcal{D}$ is defined by

$$\mathcal{D} = \frac{M_t}{(1-e^2)^{3/2}} \frac{d}{dt} \,. \tag{S37}$$

Adding resonance locking effect, these equations should be modified as

$$\mathcal{D}y = \mathcal{D}^0 y + \mathcal{D}^1 y \,, \tag{S38}$$

$$\mathcal{D}e^2 = \mathcal{D}^0 e^2 + \mathcal{D}^1 e^2 \,, \tag{S39}$$

where $\mathcal{D}^0$ terms are given by Eqs. (S33) and (S34). Since the locking occurs at very low y, we consider only the Newtonian-order contribution to $\mathcal{D}^1$. At Newtonian order, the energy and angular momentum of a spin-orbit locked system are given by

$$E = -\frac{\mu}{2} y^2 (1-e^2) + \frac{1}{2} \frac{I}{M_t^2} y^6 (1-e^2)^3 \,, \tag{S40}$$

$$L = \mu M_t y^{-1} + \frac{I}{M_t} y^3 (1-e^2)^{3/2} \,, \tag{S41}$$

and the energy and angular momentum losses caused by gravitational wave radiation are [102]

$$\frac{dE}{dt} = -\frac{32}{5} \frac{\mu^2}{M_t^2} y^{10} (1-e^2)^{3/2} \left(1 + \frac{73}{24} e^2 + \frac{37}{96} e^4 \right) , \tag{S42}$$

$$\frac{dL}{dt} = -\frac{32}{5} \frac{\mu^2}{M_t} y^7 (1-e^2)^{3/2} \left(1 + \frac{7}{8} e^2 \right) . \tag{S43}$$

Combining Eqs. (S40-S43), we get the correction as

$$D^1 y = \nu y^{13} c_0 \frac{3(1-e^2)^{1/2} I}{\mu M_t^2 - 3(1-e^2)^2 I y^4} \,, \tag{S44}$$

$$D^1 e^2 = -\nu y^{12} c_0 \frac{6(1-e^2)(1-e^2-\sqrt{1-e^2}) I}{\mu M_t^2 - 3(1-e^2)^2 I y^4} \,, \tag{S45}$$

where

$$c_0 = a_0 (1-e^2) + \frac{b_0}{2} \,. \tag{S46}$$

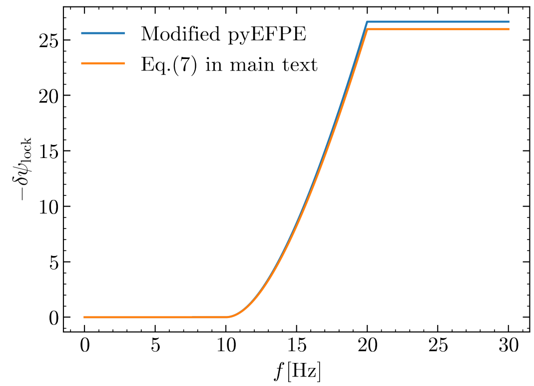

FIG. S7. Phase correction obtained from the modified PYEFPE model for a non-eccentric binary merger, with $M = M' = 1.4\,M_\odot$. The locking start from 10 Hz and break at $f_{\rm br} = 20$ Hz. The result is compared with the phase correction for circular orbits, Eq. (7), derived in the main text.

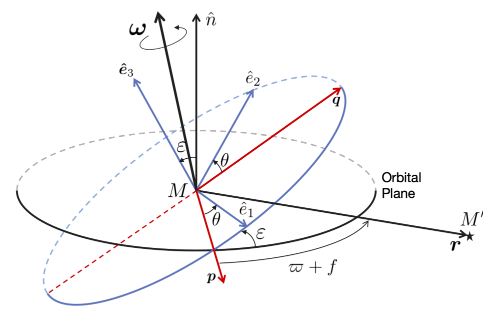

FIG. S8. The geometry and the motion of a deformed star M in the body frame and orbital plane, with the companion M' being located at $\boldsymbol{r}$. $\boldsymbol{\omega}$ is the angular velocity. $\hat{\boldsymbol{e}}_1$, $\hat{\boldsymbol{e}}_2$ and $\hat{\boldsymbol{e}}_3$ are the three unit eigenvectors along the principal axes of moment of inertia. $\hat{\boldsymbol{n}}$ is a unit vector normal to the orbital plane. $\boldsymbol{p}$ denotes the direction of equinox. θ is the angle between $\boldsymbol{p}$ and $\hat{\boldsymbol{e}}_1$ and $\varpi + f$ is the angle between $\boldsymbol{p}$ and $\boldsymbol{r}$, where f is the true anomaly and ϖ is the longitude of periapsis. ε is the angle between $\hat{\boldsymbol{n}}$ and $\hat{\boldsymbol{e}}_3$.

We incorporated this correction to the equations of motion into the PYEFPE waveform model. Figure S7 shows the phase correction obtained from the modified PYEFPE model for a non-eccentric binary, compared with the phase correction for the circular orbit derived in the main text [cf. Eq. (7)]. It can be seen that both corrections are consistent. When searching in GW200105 data, we used this modified PYEFPE model.

GENERAL CASE FOR SPIN-ORBIT RESONANCE

For a deformed neutron star, we denote the three unit eigenvectors along the principal axes as $\hat{\boldsymbol{e}}_1$, $\hat{\boldsymbol{e}}_2$ and $\hat{\boldsymbol{e}}_3$, with corresponding eigenvalues I_1, I_2 and I_3. The angular velocity is $\boldsymbol{\omega} = \omega_1\hat{\boldsymbol{e}}_1 + \omega_2\hat{\boldsymbol{e}}_2 + \omega_3\hat{\boldsymbol{e}}_3$. We illustrate the geometry and the motion of the neutron star in Fig. S8. In general, the spin vector $\boldsymbol{\omega}$ does not coincide with the principal axes. Additionally, $\boldsymbol{\omega}$ also does not need to align with the orbital normal $\hat{\boldsymbol{n}}$. These features result in more complex dynamics of the neutron star, including two types of precession: one is the precession of $\boldsymbol{\omega}$ about the normal to the orbital plane with rate $\Omega_{p,1} \sim \epsilon n^2/\omega$, and the other is the precession of $\hat{\boldsymbol{e}}_3$ about $\boldsymbol{\omega}$ with rate $\Omega_{p,2} \sim \epsilon\omega$. Near the resonance, we have $\omega \simeq n$, therefore both two precessions have a timescale of roughly $1/(\epsilon n)$, which is much longer than the resonance timescale $\sqrt{1/\dot{n}}$ for $\epsilon \lesssim 10^{-4}$. In the following discussion, we will neglect the precessions due to their relatively long timescales. A detailed study of the precessions may be pursued in future work.

We work in the body frame $(\hat{\boldsymbol{e}}_1, \hat{\boldsymbol{e}}_2, \hat{\boldsymbol{e}}_3)$. The Euler's equations of motion are

$$I_1\dot{\omega}_1 - (I_2 - I_3)\omega_2\omega_3 = N_1\,, \tag{S47}$$
$$I_2\dot{\omega}_2 - (I_3 - I_1)\omega_3\omega_1 = N_2\,, \tag{S48}$$
$$I_3\dot{\omega}_3 - (I_1 - I_2)\omega_1\omega_2 = N_3\,, \tag{S49}$$

where the gravitational torques received by the companion are [54]

$$N_1 = \frac{3GM'}{r^3}(I_3 - I_2)(\hat{\boldsymbol{r}}\cdot\hat{\boldsymbol{e}}_2)(\hat{\boldsymbol{r}}\cdot\hat{\boldsymbol{e}}_3)\,, \tag{S50}$$
$$N_2 = \frac{3GM'}{r^3}(I_1 - I_3)(\hat{\boldsymbol{r}}\cdot\hat{\boldsymbol{e}}_3)(\hat{\boldsymbol{r}}\cdot\hat{\boldsymbol{e}}_1)\,, \tag{S51}$$
$$N_3 = \frac{3GM'}{r^3}(I_2 - I_1)(\hat{\boldsymbol{r}}\cdot\hat{\boldsymbol{e}}_1)(\hat{\boldsymbol{r}}\cdot\hat{\boldsymbol{e}}_2)\,. \tag{S52}$$

Note we have

$$\begin{cases} \hat{\boldsymbol{r}}\cdot\hat{\boldsymbol{e}}_1 = \cos w\cos\theta + \sin w\sin\theta\cos\varepsilon\,, \\ \hat{\boldsymbol{r}}\cdot\hat{\boldsymbol{e}}_2 = -\cos w\sin\theta + \sin w\cos\theta\cos\varepsilon\,, \\ \hat{\boldsymbol{r}}\cdot\hat{\boldsymbol{e}}_3 = -\sin w\sin\varepsilon\,, \end{cases} \tag{S53}$$

where $w = \varpi + f$. Plugging Eq. (S53) into Eqs. (S50-S52) we get

$$\begin{aligned} N_1 =&\frac{3GM'}{2r^3}(I_3 - I_2)\Big[\sin(\theta - 2w)\cos^2\frac{\varepsilon}{2}\sin\varepsilon \\ &- \sin(\theta + 2w)\sin^2\frac{\varepsilon}{2}\sin\varepsilon - \frac{1}{2}\sin\theta\sin 2\varepsilon\Big]\,. \end{aligned} \tag{S54}$$
$$\begin{aligned} N_2 =&\frac{3GM'}{2r^3}(I_1 - I_3)\Big[\cos(\theta - 2w)\cos^2\frac{\varepsilon}{2}\sin\varepsilon \\ &+ \cos(\theta + 2w)\sin^2\frac{\varepsilon}{2}\sin\varepsilon - \frac{1}{2}\cos\theta\sin 2\varepsilon\Big]\,. \end{aligned} \tag{S55}$$
$$\begin{aligned} N_3 =&-\frac{3GM'}{2r^3}(I_2 - I_1)\Big[\sin(2\theta - 2w)\cos^4\frac{\varepsilon}{2} \\ &+ \sin(2\theta + 2w)\sin^4\frac{\varepsilon}{2} + \frac{1}{2}\sin 2\theta\sin^2\varepsilon\Big]\,. \end{aligned} \tag{S56}$$

We now consider that the rotation frequency $\omega_3 = \dot{\theta}$ and the mean motion $n = \dot{\ell}$ are close to resonance ($\omega_3 \simeq pn$). By doing average over one orbital period and retaining all the terms with argument $2(\theta - p\ell)$, we then obtain the average torque [103]

$$\begin{aligned} \langle N_3\rangle = &-\frac{3GM'}{8a^3}(I_2 - I_1)\Big[(x+1)^2H(p,e)\sin 2(\theta - p\ell - \varpi) \\ &+ (x-1)^2H(-p,e)\sin 2(\theta - p\ell + \varpi) \\ &+ 2(1-x^2)G(p,e)\sin 2(\theta - p\ell)\Big]\,, \end{aligned} \tag{S57}$$

where $x = \cos\varepsilon$ and $G(p,e)$ is a power series in e. For $p = 1$ and $p = 3/2$, we have

$$G(1,e) = \frac{9}{4}e^2 + \frac{7}{4}e^4 \quad \text{and} \quad G(\frac{3}{2},e) = \frac{53}{16}e^3\,. \tag{S58}$$

Substituting Eq. (S57) into Eq. (S49), we get

$$\dot{\omega}_3 - \epsilon\omega_1\omega_2 = -\frac{\mathcal{B}_x}{2}\sin 2(\theta - p\ell - \varpi_x)\,, \tag{S59}$$

where

$$\begin{aligned} \left(\frac{\mathcal{B}_x}{\mathcal{B}}\right)^2 =&4\big[(g + h^+ + h^-)^2 - 4g(h^+ + h^-)\sin^2\varpi \\ &- 4h^+h^-\sin^2 2\varpi\big]\,, \end{aligned} \tag{S60}$$
$$\tan 2\varpi_x = \frac{(h^+ - h^-)\sin 2\varpi}{g + (h^+ + h^-)\cos 2\varpi}\,, \tag{S61}$$

with

$$\mathcal{B} = 3\epsilon n^2\frac{q}{1+q}\,, \tag{S62}$$
$$g = \frac{1}{4}(1-x^2)G(p,e)\,, \tag{S63}$$
$$h^\pm = \frac{1}{8}(x\pm 1)^2H(\pm p,e)\,. \tag{S64}$$

Let $\gamma = 2(\theta - p\ell - \varpi_x)$, then $\ddot{\gamma} = 2(\dot{\omega}_3 - p\dot{n})$, where we have neglect the slow variation of ϖ_x caused by the precessions. Thus, Eq. (S59) can be rewritten as

$$\ddot{\gamma} + \mathcal{B}_x\sin\gamma = -2p\dot{n} + 2\epsilon\omega_1\omega_2\,, \tag{S65}$$

which is the same as Eq. (4) in the main text or Eq. (S25) in the Supplemental Material. We may further use Eq. (5) to evaluate the probability of capturing into resonance. Note here ω_1 and ω_2 can be considered as constants due to the long period of precession. For example, for a circular orbit with $e = 0$, we have $g = h^- = 0$ and thus

$$\mathcal{B}_x = \frac{3}{4}\epsilon n^2\frac{q}{1+q}(1+x)^2. \tag{S66}$$

If we further assume $\epsilon\omega_1\omega_2 \ll \dot{n}$, we can get the probability as

$$\mathcal{P}(1,0) = \frac{4\sqrt{3}}{\pi}\left(\frac{q}{1+q}\right)^{1/2}\epsilon^{1/2}\frac{1+x}{2}\,, \tag{S67}$$

which is reduced by a factor of $(1+x)/2$ compared to Eq. (5).

INJECTION WITH A LOWER BREAKING FREQUENCY OF $f_{\rm br} = 10\,\mathrm{Hz}$

In this section, we inject locking signals with a lower breaking frequency of $f_{\rm br} = 10\,\mathrm{Hz}$. Figure S9 shows the posterior distributions of the breaking frequency $f_{\rm br}$ and the moment of inertia I for the different injections. The figure shows that A+ either fails to recover the injected values or does so poorly, whereas the CE+ET network recovers the values accurately.

SEARCH IN GW190814

In this section, we present some details of the search in GW190814. First, due to noise caused by thunderstorm in the Livingston data, which affects frequencies up to 30 Hz, we follow LIGO's approach and use a starting frequency of 30 Hz to analyze the LIGO Livingston data. Second, because GW190814 is a system with an extreme mass ratio ($q \approx 9$), it exhibits stronger evidence for higher-order multipoles. Therefore we choose the IMRPhenomXPHM waveform [67] as the baseline waveform. The phase correction derived in the main text only applies to the $(\ell, m) = (2, 2)$ multipole, and for higher-order multipoles, we take

$$\delta\psi_{\ell m}(f) = \frac{m}{2}\delta\psi_{22}(\frac{2}{m}f)\,, \tag{S68}$$

where $\delta\psi_{22}(f)$ is given by Eq. (7) in the main text. We include $(2, 2)$, $(3, 3)$, $(2, 1)$ and $(4, 4)$ modes in the analysis.

Third, during the search, we set a uniform prior for the moment of inertia (I), but we also impose a constraint of $I/M^3 > 4$, where the value of 4 corresponds to the Schwarzschild black hole limit. In Fig. S10, we plot the full posterior distribution of parameters for GW190814 with Hanford-Livingston-Virgo data.

NSBH POPULATION

In order to calculate how many NSBH merger events with locking can be resolved by CE+ET, we performed a population analysis. In this section, we provide a detailed description of our population model. For the black hole mass, we take a power-law distribution with a spectral index of 2.7, featuring a sharp cutoff at the lower end of $4\,M_\odot$ and an upper bound of $40\,M_\odot$:

$$p(m_{\rm BH}) \propto \begin{cases} m_{\rm BH}^{-2.7}\,, & 4\,M_\odot < m_{\rm BH} < 40\,M_\odot\,, \\ 0\,, & \text{otherwise}\,. \end{cases} \tag{S69}$$

For the neutron star mass, we assume a uniform mass distribution between $1.1\,M_\odot$ and $2.1\,M_\odot$, i.e., $p(m_{\rm NS}) \sim \mathrm{U}(1.1\,M_\odot, 2.1\,M_\odot)$. For simplicity, we do not consider black hole spin in this analysis. We also take a volumetric NSBH merger rate with locking signal as

$$\mathcal{R}(z) = \mathcal{R}_{\rm lock} \times (1+z)^{3.2} e^{-z^2/3}\,, \tag{S70}$$

where the exponent 3.2 is taken from the redshift dependence for the BBH merger rate inferred in GWTC-4 [87], and the factor $e^{-z^2/3}$ accounts for the suppression at high redshifts. We assume a flat ΛCDM cosmology with $H_0 = 67.4\,\mathrm{km\,s^{-1}\,Mpc^{-1}}$ and $\Omega_m = 0.315$ [104].

For each choice of ϵ, we evaluate the corresponding breaking frequency $f_{\rm br}$ for the population, and assume locking signal can be resolved by CE+ET if the accumulated SNR in the frequency band $[1\,\mathrm{Hz}, f_{\rm br}]$ exceeds the threshold $\rho_{\rm thr} = 10$. This allows us to calculate the fraction of resolvable events as a function of redshift, i.e., $f_{\rm res}(z)$. Then we get the resolvable merger events

$$\dot{N}_{\rm res} = \int \frac{dV_c(z)}{dz}\frac{\mathcal{R}(z)}{1+z} f_{\rm res}(z) dz\,. \tag{S71}$$

In Fig. S11, we show the distribution of $d\dot{N}_{\rm res}/dz$ as a function of redshift z for different values of ϵ.

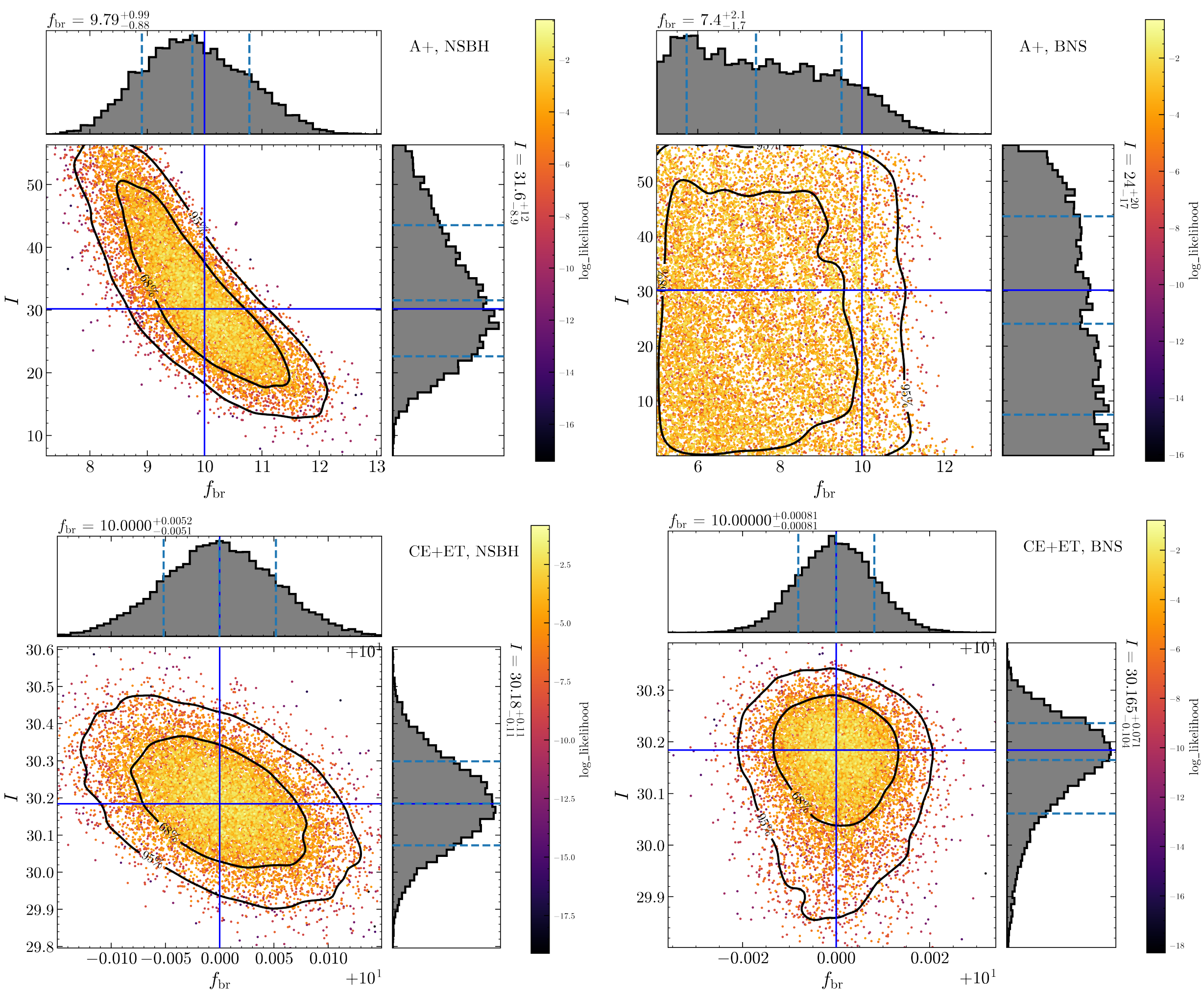

FIG. S9. Same as Fig. 3 in the main text, but for injections with $f_{br} = 10\,\mathrm{Hz}$.

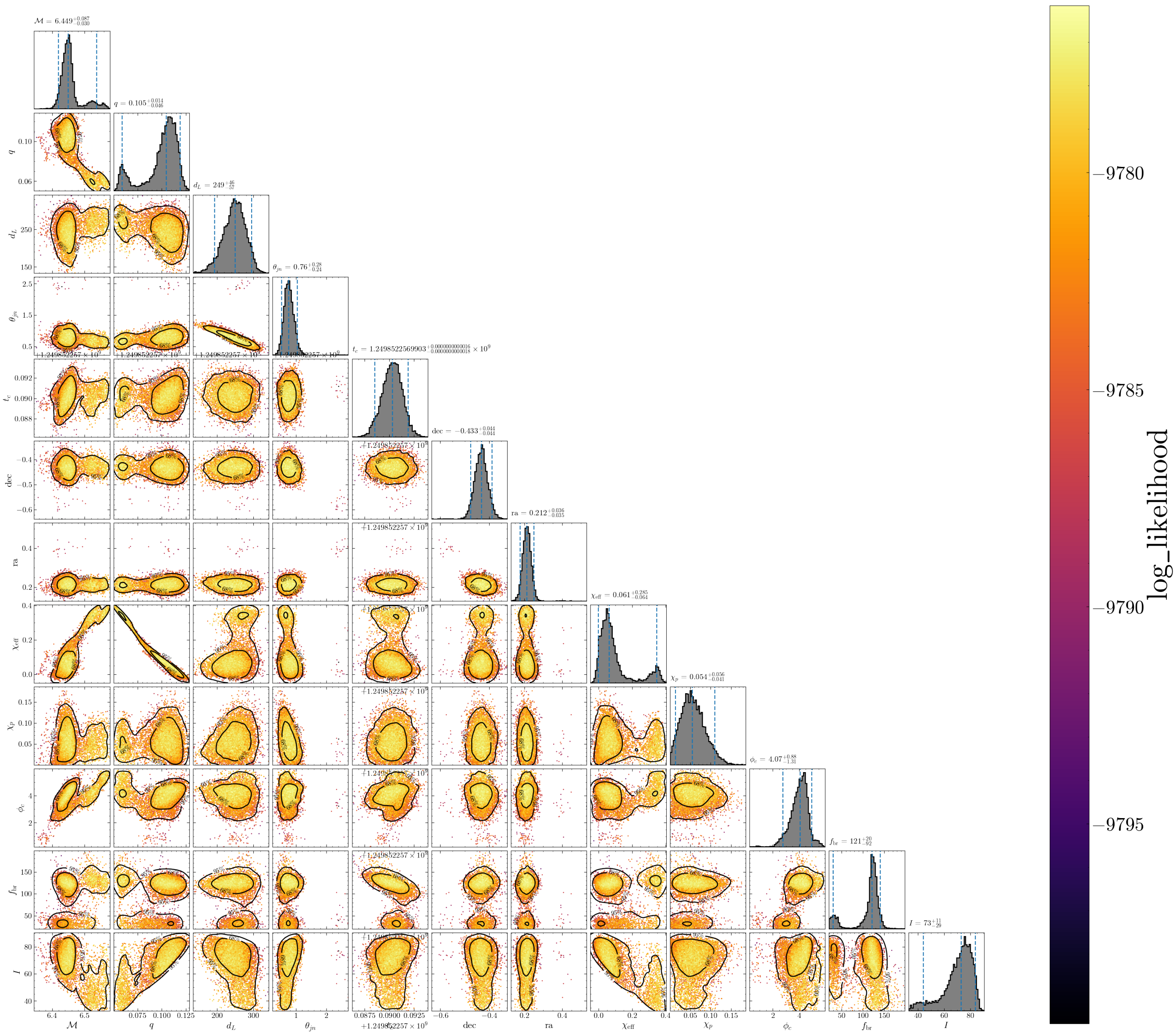

FIG. S10. The posterior distribution of all parameters in the search of resonance locking presented in Fig. 5 in the main text with data from GW190814.

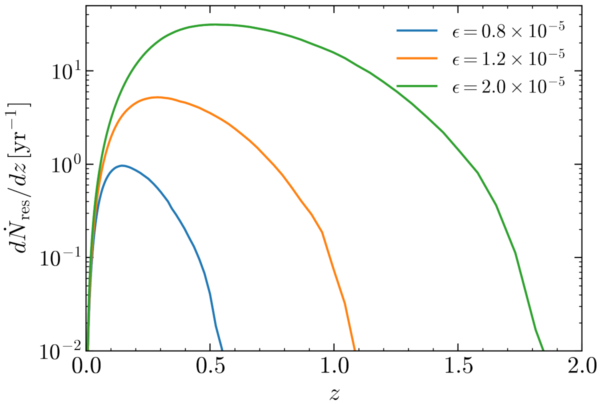

FIG. S11. Detection rate as a function of redshift z for different ϵ. The results shown in the figure are assuming a magnetar fraction of $f_{\rm mag} = 1$ in NSBH binaries.